JOURNAL OF SPACECRAFT AND ROCKETS
Vol. 35, No. 1, January–February 1998

Pressure Measurements on a Mach 5 Sabot During Discard

Jason N. Dick* and David S. Dolling†
University of Texas at Austin, Austin, Texas 78712

An experimental program has been conducted in a Mach 5 airflow to obtain surface pressures in the scoop and on the underside of a sabot at different stages of the discard process. The data are needed to validate computer codes used for predicting the trajectory of the sabot during discard and to aid in the design of minimum-interference sabots. Because of wind-tunnel size constraints, the tests were carried out using a model with one sabot petal. The remaining sabot petals were modeled by using splitter plates as symmetry planes. Assessment of the data indicates that the complex flow structure between the sabot and projectile is simulated using this approach. Because of the complex shock–shock and shock–boundary-layer interactions, the pressure distributions on the sabot underside have very distinctive shapes with large maxima; if a code can locate these maxima and predict their magnitudes reasonably well, then the integrated forces and moments (which determine the sabot trajectory) should be modeled reasonably accurately. The current data should prove useful in that regard.

Nomenclature

d = diameter of projectile, in. (cm)
L = overall length of sabot, in. (cm)
M = Mach number
P = pressure, psi (N/m^2)
S = sabot body coordinate, in. (cm)
T = temperature, °R (K)
X, Y = coordinates relative to projectile base (see Fig. 4), in. (cm)
β = shock wave angle, deg
Δy = vertical gap between top of projectile and back of sabot, i.e., in Y-axis direction, in. (cm)
δ = boundary-layer thickness, in. (cm)
θ = flow deflection angle, deg

Subscripts

static = static value of the freestream flow
w = value at the surface of the sabot
0 = stagnation value
1 = freestream value, value upstream of normal shock
2 = value downstream of normal shock

Introduction

CURRENT design practice for antiarmor kinetic-energy projectiles requires a sabot for the launch from the gun. These projectiles are typically long, slender bodies, which are fin stabilized during flight, and the sabot provides the structural support needed to prevent buckling of the projectile during the launch. In addition, within the bore the sabot also provides gas sealing and reduced sectional density. Upon leaving the barrel of the gun the sabot, usually consisting of three or four petals, breaks away from the projectile, thereby allowing the projectile to continue on in low-drag flight. The sabot discard process is a result of the action of elastic, inertial, and aerodynamic loads,[1–6] and during this process, aerodynamic interference between the sabot petals and the projectile may perturb its trajectory.[1,3,6] To minimize such interference, various sabot configurations are being designed and tested by the U.S. Army to examine their effectiveness in reducing the perturbation to the projectile.

In an effort to predict the sabot discard process and to aid in the design of a low-interference sabot, AVCO Systems Division developed a computer model.[2–5] The AVCO code is limited to relatively simple geometries, and an effort is being made at the Institute for Advanced Technology (IAT) at the University of Texas at Austin to update this code for more complex geometry sabots.[7,8] IAT is modifying the original AVCO code to predict the trajectory of the sabot during discard. To evaluate this approach, projectile-sabot launches are being made with a two-stage light gas gun at IAT. X-ray and witness plate techniques provide radial and angular displacement at specific downrange locations and are being used for comparison with the predictions of the modified AVCO code. To determine the sabot trajectory, this code relies on predicted surface pressures.[7,8] IAT is developing computational fluid dynamics (CFD) programs to predict the surface pressures on the sabot. However, the advanced geometry of the sabots being tested by IAT requires that the validity of the predicted pressure be checked by comparisons with experimental pressure distributions in the front scoop and along the underside of the sabot.

In earlier experimental work, Schmidt[6] measured pressure distributions on a generic sabot/projectile at Mach 4.5 in one of the NASA Langley Research Center facilities. Three-dimensional, laminar, Navier–Stokes computations by Nusca[9,10] in 1990 and 1991 compared favorably with the pressure measurements on both the projectile and sabot surfaces. Lesage and Raw[11] also computed pressure distributions for Schmidt's configuration (as well as other external ballistics configurations) using a Navier–Stokes code and captured the basic trends of the pressure distribution on the sabot centerline. Because Schmidt's sabot had a very simple geometry and the tests were conducted at a relatively low Reynolds number (6.6×10^6 m^{-1}), the data are of limited value to the current study. In a more recent experiment by Lesage and Girard,[12] a geometry similar to that used by Schmidt was tested, at Mach numbers of 3.5 and 4.0. In addition, surface pressures were obtained on a full-scale, antitank penetrator projectile-sabot. Overall there was reasonable agreement between experiment and computation. However, in both cases the geometry was significantly simpler than the sabots under investigation by IAT.

Because of the limited size of the wind-tunnel test section at the University of Texas, an experimental setup similar to Schmidt's was used. Because it was not practical for Schmidt to use multiple actuated sabot components, he devised a method that simulated the flowfield by using only one driven sabot segment and splitter plates as reflecting planes of symmetry for the trilaterally symmetric flow. The approach was validated by comparing results with splitter plates obtained at a specific point in the sabot discard process with a test

Presented as Paper 96-2042 at the AIAA 27th Fluid Dynamics Conference, New Orleans, LA, June 17–20, 1996; received Feb. 6, 1997; revision received June 25, 1997; accepted for publication July 15, 1997.

*Graduate Student, Department of Aerospace Engineering and Engineering Mechanics; currently Aerospace Engineer, Waco Operations, Raytheon E-Systems, Waco, TX 76710.

†Professor, Department of Aerospace Engineering and Engineering Mechanics. Associate Fellow AIAA.

including all three sabot petals fixed at the same discard point. The pressure distributions measured on the projectile and sabot component agreed qualitatively quite well in both cases, and there were only small differences in the locations of the primary flow structures. However, the pressure levels were slightly different for the two tests and were assumed to be due to the viscous effects associated with the splitter plates. The plates have boundary layers, and at their intersection with the projectile, a corner flow develops. Schmidt concluded, "while exact quantitative agreement is not arrived at due to greater viscous interactions observed with the splitter plates installed, sufficiently good qualitative comparison is developed to conclude that the test technique is valid within the approximations and limitations of any scale model wind tunnel experiment."[6] On that basis, a similar approach was adopted in the current work.

Note that the ultimate goal of this work is the accurate computation of the sabot trajectory. The latter depends on the integrated forces and moments that act on the sabot, and these are, in general, relatively insensitive to details in the pressure distributions. Significant discrepancies in predicting a sharp local pressure peak may have little effect on the integrated force or moment.

Experimental Program

Wind Tunnel and Model Design

The tests were conducted in the Mach 5 blowdown wind tunnel of the University of Texas at Austin. The tunnel has a freestream Mach number of 4.95 at the nozzle exit. The test section of the wind tunnel measures 7 in. (17.8 cm) high by 6 in. (15.2 cm) wide with a length of 27 in. (68.6 cm). The air used in the wind tunnel is compressed by a Worthington four-stage compressor and stored at ambient temperature at a maximum pressure of 2550 psig (17.6×10^6 N/m^2). Nominal stagnation pressures and temperatures for all tests were $P_0 = 335 \pm 5$ psia ($2.31 \pm 0.03 \times 10^6$ N/m^2) and $T_0 = 630 \pm 10$°R (350 ± 6 K), respectively. With these nominal conditions, the freestream Reynolds number was 15.9×10^6 ft^{-1} (52.1×10^6 m^{-1}).

The sabot used is designated by IAT as the four-petal HVP_94_016 model (Fig. 1). The sabots used by IAT in their tests are scaled down to the bore size of their two-stage light gas gun. The sabot used in the present study had the same geometry but was modified on the upper external surface to simplify instrumentation installation. Because the wind tunnel has a 7×6 in. (17.8×15.2 cm) test section, it was only feasible to model part of the entire sabot-projectile assembly. Therefore, as noted earlier, a setup similar to that used by Schmidt[6] was used. Figure 2 shows a schematic of the model setup in the tunnel test section. For clarity, the splitter plates are not shown.

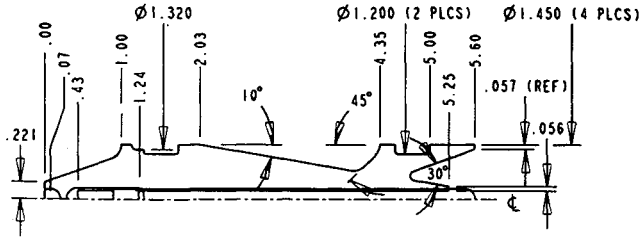

Fig. 1 IAT HVP_94_016 four petal sabot; flow is from right to left.

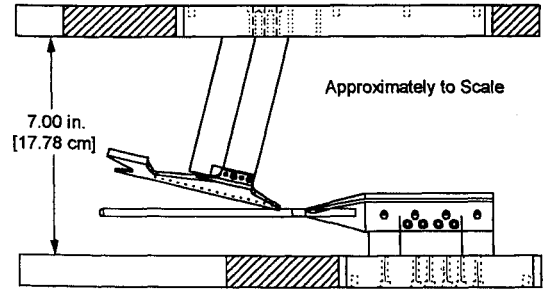

Fig. 2 Wind-tunnel test section for sabot at 14-deg AOA (splitter plates not shown).

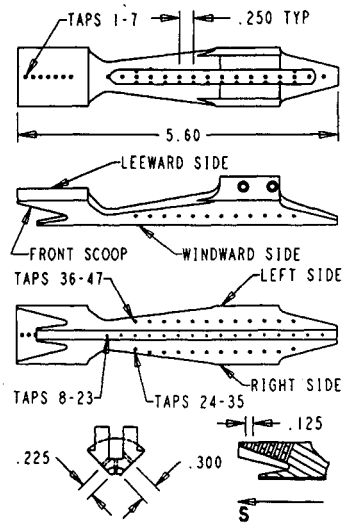

Fig. 3 One-quarter petal sabot modified for wind-tunnel mounting and for static pressure orifices; flow is from left to right.

The 90-deg included angle sabot component is mounted on a sting attached to the ceiling of the test section, and the projectile and splitter plates are mounted on a sting attached to the test section floor. The positions of the projectile and splitter plates can be adjusted independently by sliding them fore or aft in the lower support and securing them with set screws. The one-quarter sabot petal was fabricated from brass, and the modifications on its outer surface were made to accommodate the stainless-steel pressure tubing and to provide an attachment point for its sting. Because the areas of interest on the sabot are the front scoop and underside, it was anticipated that these modifications (on the top and toward the rear) would not result in interference to those areas.

Figure 3 shows the locations of the 47 static pressure taps: 7 taps were placed in the front scoop (taps 1–7), 16 were placed on the centerline on the underside (taps 8–23), and two rows of 12 each were located at different radial positions along the left (taps 36–47) and right (taps 24–35) sides. On the left side the taps are 0.225 in. (0.57 cm) from the underside edge of the sabot. On the right side, with the exception of the first and last taps, the taps are 0.300 in. (0.76 cm) from the underside edge of the sabot. The first and last taps were placed 0.225 in. (0.57 cm) from the underside edge, the same as on the left side. The purpose of having two taps at the same radial location on both sides was to determine whether the sabot is yawed with respect to the freestream flow. The radial positions of 0.225 in. (0.57 cm) and 0.300 in. (0.76 cm) are the minimum and maximum locations that allow the pressure tubing to be taken out of the upper slot on the sabot.

The static pressure taps were connected to 0.050-in. (0.13-cm) stainless-steel tubing, which was used to take the pressures out of the wind-tunnel test section. Nylon tubing was then used to connect to a Scanivalve with a 50 psia (3.45×10^5 N/m^2) differential pressure transducer installed inside it. A LeCroy data acquisition system, controlled by a Hewlett–Packard workstation, was used to record the data.

The projectile was also fabricated from brass and has a diameter of 0.250 in. (0.64 cm) with a hemispherical nose, which is the projectile configuration used by IAT in their tests. The splitter plates have an externally beveled leading edge with a 7-deg angle and to withstand aerodynamic loads, especially during startup, are made from 0.125-in. (0.32-cm) stainless-steel plates. The sides facing the sabot are polished, and the splitter plates are positioned 90 deg apart.

Test Program

The experimental program involved four distinct configurations, which are identified by the sabot's angle of attack (AOA) and vertical separation distance from the projectile (Table 1). Figure 4 shows the coordinate system, which is fixed to the projectile with the origin at the base of the upper edge of the projectile. The vertical separation distance is given by Δy (Fig. 4), whereas AOA is determined relative to the freestream velocity vector. The sabot's body coordinate system has its origin at the sabot's rear underside edge and is the coordinate system that is used to present the results.

Table 1 Sabot discard points used in experiments

AOA, deg	Y, in. (cm)
3	0.03 (0.08)
7	0.03 (0.08)
14	0.20 (0.51)
23	0.03 (0.08)

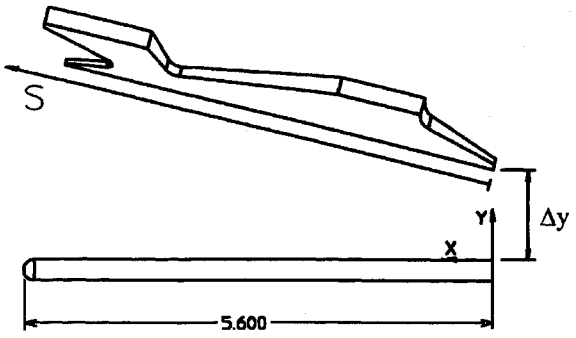

Fig. 4 Coordinate system of experimental setup.

Each AOA and corresponding vertical separation employed a separate sting. In addition, because it was uncertain how well the splitter plates would model the shocks generated by the missing sabot petals, a number of tests with the splitter plates at different axial positions relative to the projectile nosetip were performed for each angle.

Results

Splitter plates were used as symmetry planes to account for the effects of the missing three sabot petals. As noted earlier, Schmidt used a similar arrangement and obtained results that were qualitatively correct and very close quantitatively to results obtained without splitter plates.[6] However, the experiments of Ref. 6 were conducted in a much larger facility [test section of 4×4 ft (1.2×1.2 m)], with a much larger sabot and projectile than in the present study. The splitter plates were smaller relative to the projectile diameter ($d/8$) than in the present study ($d/2$), where d is the diameter of the projectile. This larger relative scale is necessary to withstand aerodynamic loads, especially during startup.

To address the question of whether the splitter plates act as symmetry planes with slight viscous effects or whether they significantly alter the flow, experiments were performed in which the axial location of the splitter plates was varied. In the ideal case, the reflected waves correspond to the waves that would have been generated by the missing sabot petals. Therefore, varying their axial position should not affect the sabot underside pressures as long as they are still reflecting the shock waves generated by the front scoop. Results of these tests will be presented later in this section.

Uncertainties in the measurements are due to a number of causes. The repeatability of the Scanivalve pressure transducer is 0.05% of full scale. The deviation of the transducer calibration line from the calibration data points was at maximum 0.3% of the fitted value. The major contribution to the uncertainties in the measurements is drift in the calibration from one test to another. When the repeatability is examined, it is found that a particular data point can shift by up to 0.7% of full scale. The full-scale pressures are typically found in the front scoop of the sabot and, thus, the uncertainty there is of order 1%. In the worst case, for the lower pressures typically found on the underside of the sabot, this shift corresponds to a maximum uncertainty of about 7%.

Sabot Only

The one-quarter petal sabot was first tested alone to obtain data on its free-flight behavior. These tests were also performed to determine whether the sabot was yawed with respect to the freestream flow. As the AOA of the sabot increases, the pressures on its underside increase (as shown in Fig. 5). The horizontal lines shown in Fig. 5 correspond to the pressure ratio through a conical shock with cone half-angles equal to each AOA. The measured pressure ratios for the angles of attack of 3, 7, and 14 deg remain fairly constant along

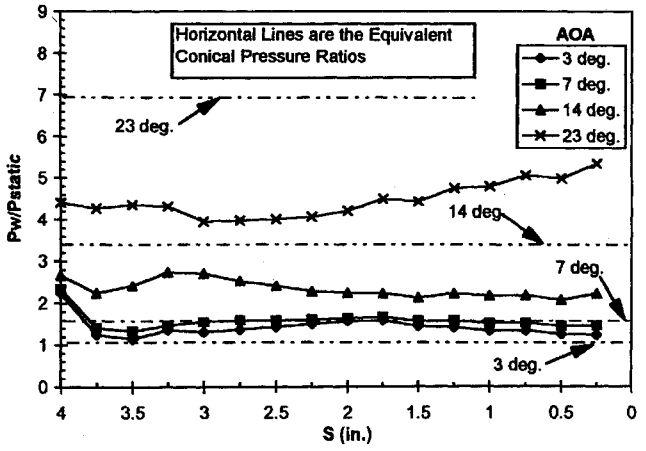

Fig. 5 Sabot in free flight, underside centerline pressures.

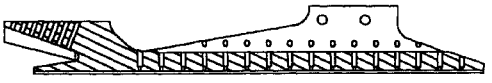

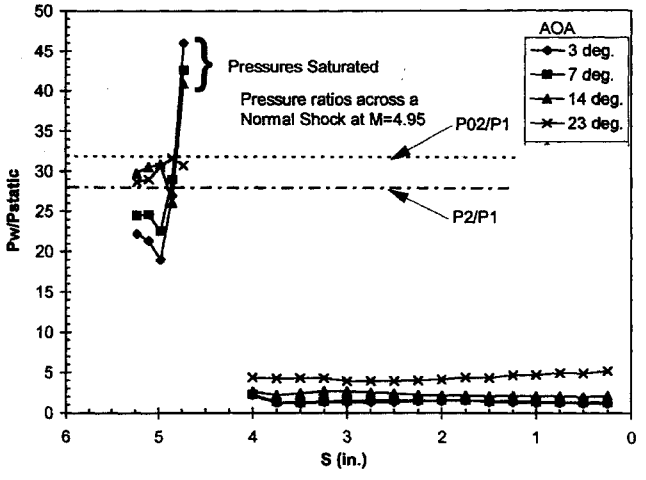

Fig. 6 Centerline pressures for sabot in free flight at four AOAs.

the undersurface although their magnitudes are lower than the conical pressure ratios because the flow is highly three dimensional and flow relief occurs very rapidly. The lower magnitudes show that the geometry of the model is too complex for simple methods to yield useful results. The measured pressure ratios for the sabot at 23-deg AOA increase at the aft end of the sabot, which is unexpected behavior but might be the result of shock–boundary-layer interaction on the tunnel floor.

The behavior of the pressures in the front scoop is more complex. Two-dimensional shock/expansion theory suggests that, because the leading edges of the borerider (upper portion of front scoop) and lower ramp are not sharp [$\approx$0.057 in. (0.14 cm)], the shocks are detached. The shocks should then be swept back at approximately the angle corresponding to the equivalent two-dimensional wedge, culminating in a series of shock reflections off the lower ramp and upper portion of the front scoop. These reflections will compress the flow to very high pressures. However, for an AOA of 23 deg, the deflection angle of the upper portion of the front scoop corresponds to a two-dimensional wedge deflection angle of 43 deg, which is greater than the maximum deflection angle for $M = 4.95$. Therefore, it would be expected that the front scoop would generate a normal shock and the flow inside the scoop would be subsonic and no reflections would occur. These predictions are supported by the experimental data, which are shown in Fig. 6.

The pressures shown in Fig. 6 begin at pressure tap 3, which is 0.375 in. (0.95 cm) from the leading edge of the sabot [$S \approx 5.225$ in. (13.27 cm)]. This is far enough back from the leading edge that the high-pressure ratios characteristic of a detached shock cannot

be seen for the 3- or 7-deg cases. The leading-edge bluntness of the upper front scoop is small [0.057 in. (0.14 cm)], and so in a very short distance the shock is swept back to the angle that would be generated by a two-dimensional wedge, and the pressure measured does not correspond to that downstream of a normal shock. However, for the 14- and 23-deg cases, evidence of a normal shock can clearly be seen in the pressure ratio. For $M = 4.95$, the pressure ratio across a normal shock is given by $P_2/P_1 = 28.4$, which is very close to that shown in Fig. 6 for 14 and 23 deg. At 23 deg, the maximum deflection angle is exceeded and, therefore, a normal shock is generated ahead of the front scoop. Inside the scoop, as noted earlier, there is no sharp increase in pressure from shock reflections. Because the sabot is at a high AOA, the pressure taps at the back of the front scoop are measuring the stagnation pressure of the flow, and for a $M = 4.95$ flow, $P_{02}/P_1 = 32.0$, as shown by the dashed line in Fig. 6.

At 14 deg, the measured pressure ratios inside the front scoop are initially close to the normal shock value of 28.4. However, there is a sharp decrease followed by a sharp increase in the pressure, which suggests that a normal shock occurs in front of the front scoop, but it is localized to the upper portion of the front scoop as for the 3- and 7-deg tests. It appears that the normal shock is most localized for the 3-deg test, and as the sabot's AOA increases then the area affected by the local normal shock increases until the sabot reaches the maximum deflection angle of the flow. At this point the normal shock occurs ahead of the entire front scoop.

As noted earlier, the pressure inside the front scoop of the sabot can become very high due to shock reflections. The highest pressures indicated in Fig. 6 correspond to the saturation pressure of the transducer. If the pressure transducer is calibrated for the entire expected pressure range, then the uncertainty of the lower pressures on the sabot underside is increased. Because of this, the pressure transducer calibration range was chosen from 0.3 psia (2.1×10^3 N/m^2) to 28 psia (1.9×10^5 N/m^2) mainly to capture the pressures on the underside of the sabot because it was originally judged more important to determine the shock interactions that occur in this region rather than the very high pressures in the back of the scoop. However, two tests were performed for the sabot at 3-deg AOA in which separate calibrations were performed to capture accurately the pressures on the underside only and in the front scoop only. Figure 7 shows the data from these two tests, as well as the data obtained using the narrower calibration range. There is very good repeatability for the different tests. The values in the front scoop overlap, whereas the values on the underside are only slightly shifted. Because the shift is the same for all of the points, this indicates it is due to calibration drift. More importantly, the pressure ratio at the previously saturated tap is now captured and is 74, which corresponds to a static pressure of 47 psia (3.2×10^5 N/m^2). This very high pressure ratio of 74 indicates shock reflections in the front scoop.

Flow Symmetry Tests

To simulate the ideal sabot discard process, the sabot must be aligned properly with the flow. Therefore, there should be no

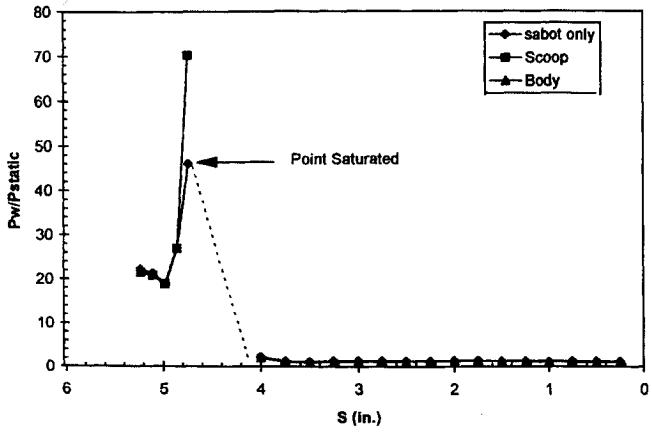

Fig. 7 Comparison of sabot-only configuration for different calibration tests.

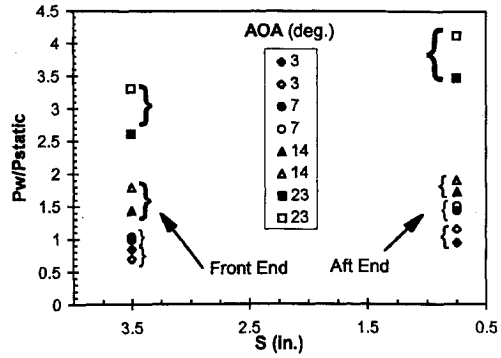

Fig. 8 Pressure tap pairs, located at 0.225 in. on each side of sabot, used for yaw analysis: closed symbol, right side and open symbol, left side.

yaw with respect to the freestream flow. Because an economical model/sting design was necessary due to budgetary constraints, the sabot is mounted on a sting that has a fixed AOA and is rigidly bolted to the tunnel ceiling. As a result, it is very difficult to make fine adjustments to the yaw angle. Therefore, it was necessary to estimate the accuracy of the test model geometry.

As noted earlier, two side pressure taps at the front and back of the sabot are positioned at the same radial locations of 0.225 in. (0.57 cm) on both the right and left sides of the sabot. If the sabot is perfectly aligned with the flow, then the pressures on the right and left sides should be the same. Figure 8 shows the pressure ratios for these pairs of corresponding taps for the four AOAs. The values are generally close but not always the same. The largest difference is 21% (at 23-deg AOA), whereas the smallest difference is 5% (at 7-deg AOA); the average is 14%. To determine how significant these percentages are in terms of model misalignment, an example of a simple plate at small AOA can be used. If the plate is at an AOA of 1 deg at $M = 4.95$, the difference between the pressures on each side will be 27%. This result shows that the pressures are very sensitive to small yaw angles. Because the measured differences are always lower than 27%, the yaw angle with respect to the freestream should be less than 1 deg for all four test cases and on average is probably around 0.5 deg. It is very close to 0 deg for the test with the sabot at 7-deg AOA.

Sabot and Projectile Only

Test cases were also run using only the sabot and projectile. The purpose was to determine the behavior without the splitter plates. Because of space constraints, only the results for the sabot at 14- and 23-deg AOA are presented in this and the following sections. The results for the remaining tests can be found in Ref. 13. Figures 9a and 10a show an analytical prediction of the shock pattern generated by the sabot-projectile system based on blast wave theory[14] and two-dimensional oblique shock wave theory. Figures 9b and 10b show the pressure distributions for the tests for the sabot/projectile combination and the sabot-alone tests.

The experimental results at 14-deg AOA, shown in Fig. 9b, support the analytical predictions shown in Fig. 9a. At this AOA, the shock generated by the lower ramp is reflected off the projectile and generates a pressure peak [at $S = 1$ in. (2.5 cm)]. The locations of this pressure peak and the peak upstream of it correspond to the analytically predicted oblique shock impingement points (as can be seen in Fig. 9).

The results at 23-deg AOA shown in Fig. 10 are harder to explain. At this high AOA, the flow deflection angle is such that a normal shock is formed. Evidence for this normal shock was presented earlier (Fig. 6). The normal shock also explains the increased pressure around $S = 2$ in. (5.1 cm), which is probably due to its reflection. The magnitude is greater than the maxima of Fig. 9, which is further evidence of a normal shock. The pressure rise at the back of the sabot is probably due to both the shock from the lower ramp and the flow choking in the narrow channel between the sabot and projectile.

The bow shock generated by the projectile does not appear to affect the pressures on the underside of the sabot. Blast wave theory

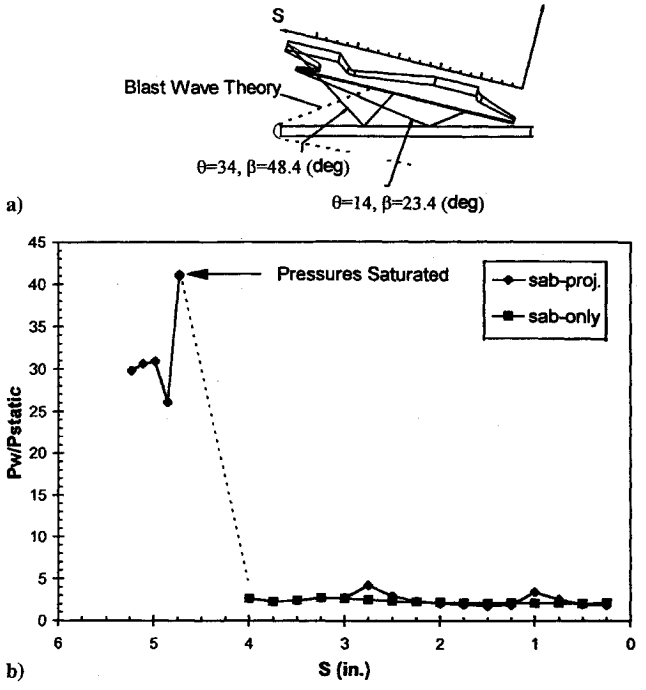

Fig. 9 Analytical prediction and experimental test results for sabot centerline pressures and for sabot at 14-deg AOA.

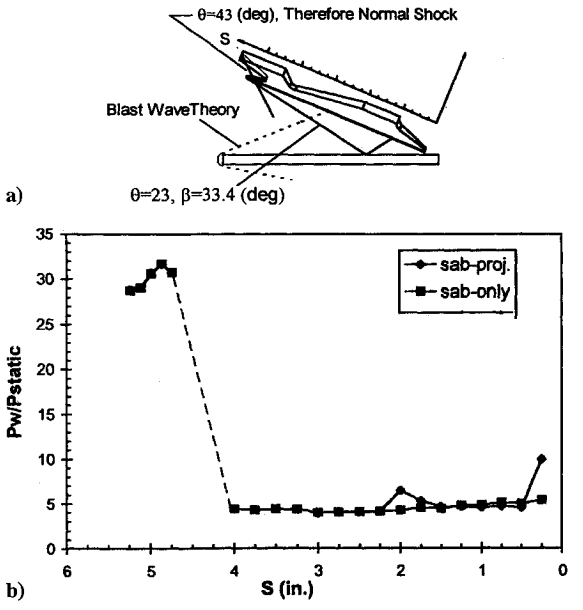

Fig. 10 Analytical prediction and experimental test results for sabot centerline pressures and for sabot at 23-deg AOA.

shown in Figs. 9a and 10a shows that the projectile bow shock impinges at a location on the sabot at which its effect should be measurable. Neither the 14- nor 23-deg test shows any effect of the bow shock. It is probable that the relieving effect of the flow greatly weakens the shock as it moves downstream so that its effects are negligible when it impinges upon the sabot.

Tests with Splitter Plates

Sabot at 23 Degrees

Results at 23-deg AOA are shown in Fig. 11. In the legend of Fig. 11, the location of the splitter plate is measured relative to the nose of the projectile. In the flush position, their leading edges are positioned at the same X coordinate as the nose of the projectile [$X = 5.6$ in. (14.2 cm)]. The 0.35-in. (0.89-cm) and 1.0-in. (2.5-cm) positions indicate that the leading edges of the splitter plates are these distances downstream of the nose of the projectile, i.e., $X = 5.25$ in. (13.3 cm) and $X = 4.60$ in. (11.7 cm).

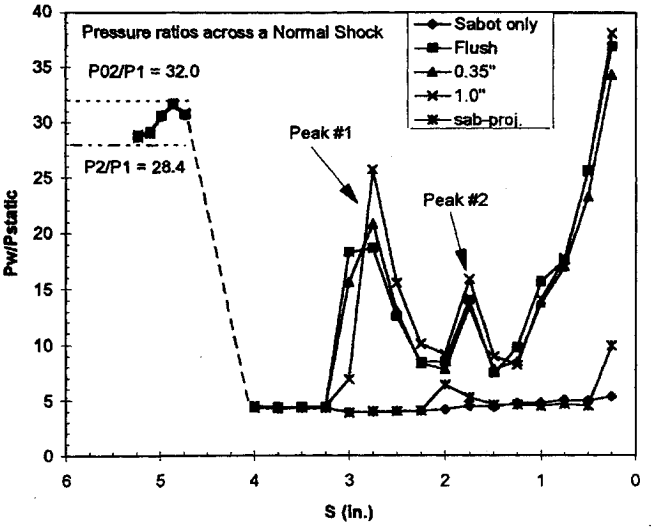

Fig. 11 Sabot centerline pressures for varying splitter plate locations and sabot at 23-deg AOA.

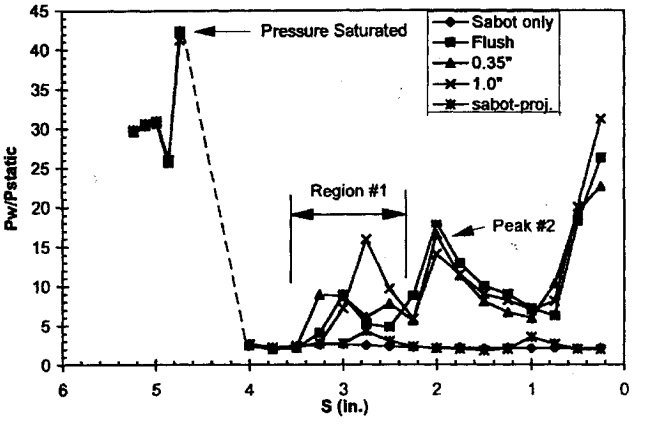

Fig. 12 Sabot centerline pressures for varying splitter plate locations and sabot at 14-deg AOA.

The simple analytical approach used to predict the flow structure shown in Fig. 10a is also useful in determining the flow structure when the splitter plates are used. Three distinct flow features on the underside of the sabot can be seen in Fig. 11. There is an initial pressure peak (peak 1), a smaller peak (peak 2), and a sharp pressure rise at the back of the sabot. Blast wave theory predicts that the bow shock of the projectile will impinge upon the sabot at approximately $S = 2.75$ in. (6.99 cm). Figure 11 shows that this is approximately the location of the beginning of peak 1. Whereas the location of peak 1 corresponds to that position predicted by blast wave theory, the very high level of peak 1 (≈20–26) suggests that it is caused by the reflection of the normal shock generated by the front scoop. The peak magnitude varies slightly with splitter plate location, but the differences are exaggerated due to the large spacing between pressure taps. If the tap resolution was refined to 0.125 in. (0.32 cm) or 0.063 in. (0.16 cm), then the location of the pressure peak could be determined more accurately. It is quite possible that the peak is shifted by less than 0.250 in. (0.64 cm) when the splitter plates are repositioned. The cause of peak 2 is harder to determine. It is either a second reflection of the front scoop normal shock or the shock generated by the lower ramp in the front scoop. The pressure rise at the back of the sabot is probably due to the flow choking as the flow area decreases.

Sabot at 14 Degrees

Pressure measurements. The results for the 14-deg AOA case present a complex picture. Figure 12 shows that there is a greater dependence on splitter plate position. The simple flow model in Fig. 9a clearly predicts the behavior for the sabot-projectile-only test but is not nearly so clear when the splitter plates are included. Based on

Fig. 9a, it would appear that pressures in region 1 are due to the reflection of the projectile bow shock and possibly the reflection of the shock generated by the upper portion of the front scoop of the sabot. Pressure peak 2 is probably due to the shock generated by the upper portion of the front scoop. The previous tests with splitter plates showed that the peaks generated by the front scoop were shifted downstream slightly, and it might be expected that the same trends would occur for the 14-deg tests. The pressure peak that is due to the lower ramp of the sabot is also probably shifted slightly downstream and, therefore, is masked by the sharp pressure rise at the back of the sabot due to the normal shock that occurs when the flow chokes.

To explore the flow structure further, more tests were conducted. These involved checking the repeatability of the data and using other splitter plate positions. The results of the tests involving additional splitter plate locations [0.125, 0.50, 0.75, and 1.5 in. (0.32, 1.27, 1.91, and 3.8 cm)] can be found in Ref. 10. The results showed that the only significant changes occurred in region 1. The effect on peak 2 of shifting the splitter plate location downstream is to reduce its magnitude and to move it slightly downstream. However, both effects were relatively small and might be mainly due to the coarseness of the pressure tap spacing.

Because each test required the removal of the lower model (projectile, splitter plates, supports) for the adjustment of the splitter plates, there was ample opportunity to examine the effects of this repositioning on the data. The results shown in Fig. 13 indicate that the differences between repeated tests are relatively small compared with the differences for different splitter plate locations.

Kerosene lampblack flow visualization. To help understand the effect of splitter plates, kerosene lampblack surface flow visualization was used. Tests were done for the splitter plates in the flush, 0.125- (0.31-), 0.35- (0.89-), and 1.0-in. (2.5-cm) positions. The results for the 1.0-in. (2.5-cm) test are presented in Fig. 14. The remaining lampblack figures can be found in Ref. 13. On the lampblack figures certain common features can be identified.

A major feature that is evident in all of the tests is the parabolic-shaped separation line that follows the shape of the reflection of the shock generated by the front scoop of the sabot. The parabolic shape indicates that the shock itself is either conical or parabolic because, when a circle or ellipse intersects a plane, a parabola is formed. Another feature is the second branch that appears on the outside edges of the splitter plates. This pattern is probably due to the shock pattern caused by the complex geometry of the front scoop. The outer edge and the lower ramp generate shocks of different strength, which result in a complex pattern on the splitter plates. On the centerline, both branches appear to merge into one shock. For this reason peak 2 of Fig. 12 is probably caused by both the upper edge shock and lower ramp shock of the front scoop. In addition, the position of this shock remains fairly constant for all of the tests, as seen in Fig. 12.

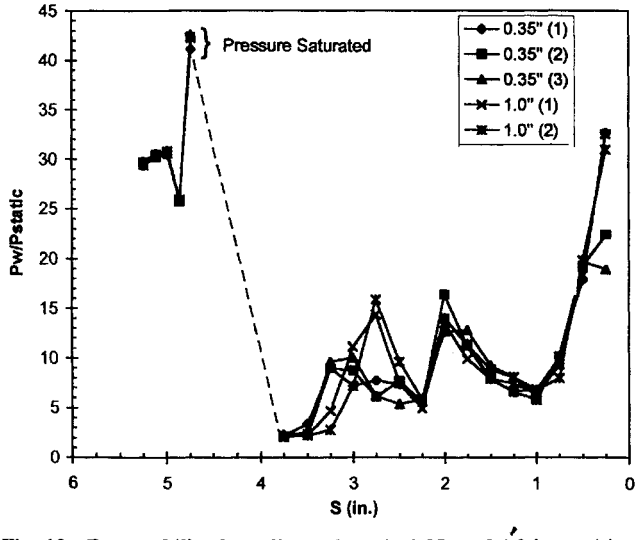

Fig. 13 Repeatability for splitter plates in 0.35- and 1.0-in. positions at 14-deg AOA.

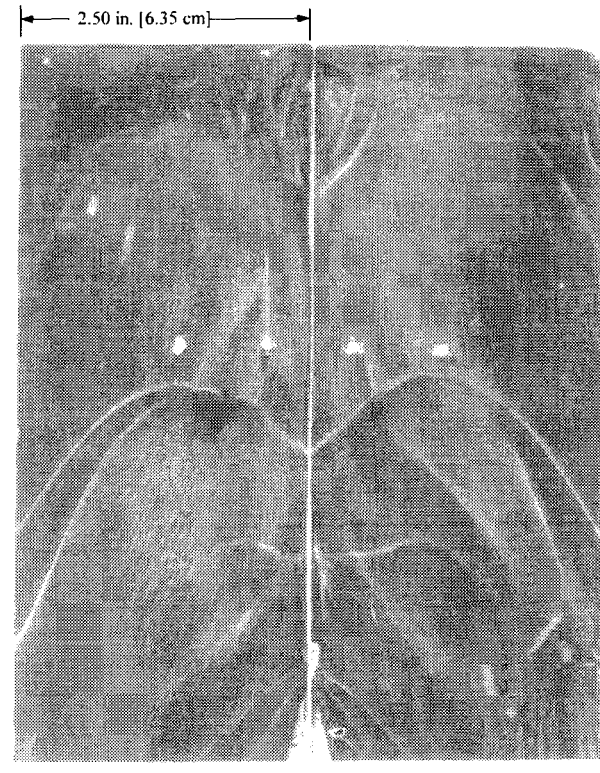

Fig. 14 Lampblack flow visualization picture for splitter plates in 1.0-in. position and sabot at 14-deg AOA; flow is from top to bottom.

Aft of the merge point of the parabolic shock pattern is another fairly constant flow feature that occurs at the sabot coordinate of approximately [$S \approx 0.3$ in. (0.76 cm)], which corresponds to the sharp pressure rise seen in Fig. 12.

Model Validity

At this point a fairly clear picture of the flow structure for the tests (sabot alone, sabot-projectile alone, and splitter plates) has been developed. The critical question is whether the flow that would occur using four sabot petals is simulated using splitter plates. The only truly definitive way to answer this question is to conduct experiments involving all four sabot petals and compare the results with the splitter plate data. Because this is not possible, the present experimental data must be used to infer an answer.

There is no question that the splitter plates must introduce disturbances into the flow. The only question concerns the nature and magnitude of the disturbances. First, note that, because the front scoop of the sabot is in freestream flow, the pressure is independent of the splitter plate location and, therefore, can be taken to be the same as for a test involving four sabot petals.

For an angle of attack of 23 deg, changing the position of the splitter plates does not have a significant effect on the underside pressures, and the flow features are clearly identifiable. The only changes are slight shifts in the location and magnitude of the features, which may be due to differences in the boundary layers on the splitter plates. When the splitter plates are moved from the flush position to the 1.0-in. (2.5-cm) position, the estimated boundary-layer thickness at $X = 0$ in. decreases by about 14%. Changes in boundary-layer thickness will affect the local shock–boundary-layer interaction and can cause the differences in the pressure data. The reflection of the front scoop shock off the projectile and splitter plates is a complex process. Any changes in boundary-layer thickness will change the shock reflection pattern and may explain the slight differences seen in the pressure data. Another possible effect is shock-induced/boundary-layer separation, which will affect the reflected shock and will contribute to differences between the present test and a test involving four sabot petals.

For the test with the sabot at 14 deg, the interference of the splitter plates is more significant. However, the only notable effect was to distort and alter the interaction of the projectile bow shock with

the sabot boundary layer. The front scoop impingement details exhibited only minor differences with splitter plate location changes. These minor differences were the same as in the tests examining data repeatability.

Overall, the splitter plates do not appear to change the fundamental structure of the flow. The question is how significantly the surface pressures are being affected. In Schmidt's study,[6] the differences varied from station to station and, in general, were approximately 20%. The maximum difference between the data with and without splitter plates occurred in the lower pressure areas and was 25%. If Schmidt's experiments are used as a guide for determining the validity of the present study, then it is necessary to understand the similarities/differences between the two experimental arrangements. One means of comparison is the ratio of boundary thickness in the gap at the aft end of the sabot to the overall length of the sabot (δ/L). This ratio is about the same in both studies (0.031 for Schmidt and 0.028 for the current arrangement). One major difference in scales between the two studies is in the normalized gap size at the aft end of the sabot (Δy). For Schmidt's study the ratio of $\delta/\Delta y$ was typically about 0.96, whereas for the present program it is about 5.2. Thus in Schmidt's experiments, there should be a very small inviscid region in the gap. Because the boundary-layer thickness in the present study is far larger than the gap size, the flow will choke sooner. In fact, Figs. 11 and 12 show that the throttling shock occurs about 1.0-in. (2.5-cm) upstream of the aft end of the sabot. Further, the pressure ratio across this throttling shock could be much greater.

Conclusions

Wind-tunnel experiments have been conducted as part of a study of sabot discard at high Mach numbers. The objective was to determine the static pressures on the sabot front scoop and underside to deduce the overall flow structure and to provide data suitable for the validation of computer codes. The two stages of the sabot discard process examined are defined by the sabot at angles of attack of 14 and 23 deg.

Because of wind-tunnel size constraints, the model was restricted to the projectile and one sabot petal only. Splitter plates were used as symmetry planes to simulate the missing petals. Experimental results show that the interference generated by the splitter plates mainly affects the bow shock generated by the projectile but is not significant enough to change the fundamental structure of the flow. Comparison of the experimental flow structure with the predictions of a simple inviscid analysis shows that the results are qualitatively correct. At the aft end of the sabot a throttling shock is present, and the pressure ratio across this shock is probably higher than for a test involving the four sabot petals because of the boundary layer due to the splitter plates.

Because of shock–shock interactions, shock–boundary-layer interactions, and the gap throttling process, the sabot pressure distributions have very distinctive shapes characterized by large pressure peaks. If a code is able to predict the locations of these features, then this is strong evidence that the essential flow structures have been captured. Even if the magnitude of the peaks is not reproduced accurately, it is unlikely that the forces and moments will be seriously in error because they are obtained through integration of surface pressures. In such a process large local errors are washed out. Thus, despite the difficulty in determining precisely the uncertainty of the present data, they should prove useful in comparisons with CFD codes.

Acknowledgment

Support for the project was provided in part by the Institute for Advanced Technology at the University of Texas at Austin, Texas, under contract to the Armament Research, Development, and Development Center.

References

[1]Schmidt, E., and Shear, D., "Aerodynamic Interference During Sabot Discard," AIAA Paper 77-1142, Aug. 1977.

[2]Siegelman, D., Wang, J., and Crimi, P., "Computation of Sabot Discard," U.S. Army Ballistic Research Lab., ARBRL-CR-00505, Aberdeen Proving Ground, MD, Feb. 1983.

[3]Siegelman, D., and Wang, J., "Sabot Design Optimization," U.S. Army Ballistic Research Lab., ARBRL-CR-00450, Aberdeen Proving Ground, MD, March 1981.

[4]Siegelman, D., and Crimi, P., "Projectile/Sabot Discard Aerodynamics," AIAA Paper 80-1588, Aug. 1980.

[5]Crimi, P., and Siegelman, D., "Analysis of Mechanical and Gasdynamic Loadings During Sabot Discard from Gun-Launched Projectiles," U.S. Army Ballistic Research Lab., CR 341, Aberdeen Proving Ground, MD, June 1977.

[6]Schmidt, E., "Wind-Tunnel Measurements of Sabot-Discard Aerodynamics," *Journal of Spacecraft and Rockets*, Vol. 15, No. 3, 1981, pp. 235–240.

[7]Guillot, M., Subramanian, R., and Reinecke, W., "A Numerical and Experimental Investigation of Sabot Separation Dynamics," Inst. for Advanced Technology, Rept. 0074, Univ. of Texas, Austin, TX, Sept. 1995.

[8]Guillot, M., and Reinecke, W., "Investigation of Pressure Distribution on Sabots in Hypervelocity Flight," AIAA Paper 96-2469, June 1996.

[9]Nusca, M., "Computational Fluid Dynamics Application to the Aerodynamics of Symmetric Sabot Discard," AIAA Paper 90-3096, Aug. 1990.

[10]Nusca, M., "Numerical Simulation of Sabot Discard Aerodynamics," AIAA Paper 91-3255, Sept. 1991.

[11]Lesage, F., and Raw, M., "Computational Fluid Dynamic Applications of a Navier–Stokes Code in External Ballistics," AIAA Paper 92-0637, Jan. 1992.

[12]Lesage, F., and Girard, B., "Wind Tunnel and CFD Investigation of Aerodynamic Interactions During Sabot Separation," AIAA Paper 96-0193, Jan. 1996.

[13]Dick, J. N., "Experimental Determination of Sabot Separation in a Mach 5 Wind Tunnel," M.S. Thesis, Dept. of Aerospace Engineering and Engineering Mechanics, Univ. of Texas, Austin, TX, May 1996.

[14]Anderson, J. D., Jr., "The Hypersonic Equivalence Principle and Blast Wave Theory," *Hypersonic and High Temperature Gas Dynamics*, McGraw–Hill, New York, 1989, pp. 117–145.

R. M. Cummings
Associate Editor